Vietnam Journal of Catalysis and Adsorption
Tạp chí xúc tác và hấp phụ Việt Nam
https://jca.edu.vn

Characteristic and CIP antibiotic and DR79 dye of lemongrass biochar derived from distillation waste

Nguyen Thi Hoa[1], Truong Thi Thao[2,*]

[1] *Thai Binh University of Medicine and Pharmacy, 373 Ly Bon, Tran Lam Ward, Hung Yen, 160000, Vietnam*
[2] *TNU-University of Sciences, Phan Dinh Phung ward, Thai Nguyen, 250000, Vietnam*
** Email: thao.tt@tnus.edu.vn*

ARTICLE INFO

Received: 17/06/2026
Accepted: 29/06/2026
Published: 30/06/2026

Keywords:
lemongrass biochar;
Ciprofloxacin;
direct red 79;
adsorption

ABSTRACT

Lemongrass residue-derived biochar was produced via pyrolysis and evaluated as a sustainable adsorbent for the removal of ciprofloxacin (CIP) and Direct Red 79 (DR79) from aqueous solutions. The physicochemical characteristics of the Biochar was investigated using SEM, BET, EDS, FTIR, and pH_{pzc} analyses. Pyrolysis at 600 °C generated a carbon-rich mesoporous material with a developed pore network, a specific surface area reaches 79.7 m^2 g^{-1}, and abundant aromatic structures while retaining oxygen-containing surface functionalities. The biochar exhibited effective adsorption toward DR79 (q_m~44 mg g^{-1}) than CIP (q_m~33 mg g^{-1}). Equilibrium data were best described by the Sips and Freundlich models, indicating adsorption on a heterogeneous surface. Kinetic studies showed that the Elovich model provided the best fit for both pollutants, while intra-particle diffusion played a more significant role in CIP adsorption. DR79 removal was mainly governed by electrostatic attraction, π–π interactions, and pore filling, whereas CIP adsorption involved hydrogen bonding, intra-particle diffusion, and aromatic interactions. These results demonstrate the potential of lemongrass residue biochar as a low-cost, eco-friendly adsorbent for the treating a wide range of organic contaminants.

Introduction

Environmental pollution remains a constant challenge for scientific research and production development today. The application of biochar derived from agricultural waste in wastewater treatment is a key research direction in environmental materials science. Biochar simultaneously addresses two pressing global challenges: sustainable biomass management and the removal of pollutants from environment [1].

Lemongrass is widely used in both culinary and cosmeceutical sectors. Its essential oil is a globally popular flavoring. The distillation process generates a continuous source of biomass - lemongrass residue (LR). Improper disposal of LR can cause foul odors, local air pollution, and greenhouse gas emissions. Therefore, converting LR into biochar is a sustainable waste utilization strategy, consistent with the principles of the circular economy. There have been several studies have utilized hydrochar derived from LR for the simultaneous treatment of heavy metals (Cr(III), Ni(II), Mn(II), Zn(II) [2]) or dyes (MB, RhB [3]). Pyrolysis is a suitable and advantageous method for converting LR into biochar. While some studies have been conducted on the preparation of Lemongrass pyrochar [4], these have primarily focused on soil improvement. Relatively few studies have examined LR as an adsorbent precursor for environmental pollution treatment.

https://doi.org/10.62239/jca.2026.033

©2026 by the authors. Licensee Vietnam Journal of Catalysis and Adsorption. This article is an open access article distributed under the terms and conditions of the Creative Commons Attribution (CC BY) license (https://creativecommons.org/licenses/by/4.0/).

Ciprofloxacin (CIP) is a second-generation, broad-spectrum fluoroquinolone antibiotic, are widely used in medicine. CIP is quite resistant to degradation, it affects aquatic organisms by altering microbial populations and disrupting ecological balance. Antibiotic residues in the environment are a significant source of the current antibiotic resistance problem, a major threat to public health [5]. Direct Red 79 (DR79) is an anionic azo dye with a complex aromatic structure, high water solubility, and strong resistance to biodegradation. Dyes can reduce light penetration in water, hinder photosynthesis, and produce toxic aromatic amines after partial degradation. Wastewater containing dyes is often inadequately treated before discharge. Adsorption is considered one of the most effective methods for antibiotic and dye removal due to its simplicity, efficiency, and adaptability to various treatment scales [6]. Numerous studies have been conducted using biochar to adsorb both antibiotics and dyes individually [5,6]. However, no studies used biochar for DR79 and CIP adsorption.

In this study, we focused on characterizing biochar derived from LR via pyrolysis for DR79 and CIP adsorption. The study contributes data on the characterization of biochar, adsorption kinetics, isothermal behavior, pH dependence, and adsorption mechanisms, aiming to a better understanding of the structure-function relationship in biomass-derived adsorbents. These insights could support future optimization of biochar for broader environmental applications.

Experimental

Chemical

Chemicals (analytical grade purity): DR79 ($C_{37}H_{28}N_6Na_4O_{17}S_4$), CIP ($C_{17}H_{18}FN_3O_3$), sodium hydroxide (NaOH), hydrochloric acid (HCl), distilled water (DW), 96% ethanol, LR (were collected from Institute of Life Sciences, Thai Nguyen University).

Method

Material Synthesis: LR were dried, then ground into fine powder. The powder was pyrolyzed under the nitrogen atmosphere at 600°C for 1 h, then cooled naturally to room temperature, washed with 0.1 M HCl then by DW untill neutral, finally dried, finely grind, and preserved in sealed plastic bags before use (LB600).

Material characterization: LB600 sample is studied some characteristics by various methods: Fourier transform infrared (FTIR, IR Spectrum Two spectrometer, Perkin Elmer (USA)); energy-dispersive X-ray spectroscopy (EDS, Jeol 6490 – JED 2300) and scanning electron microscopy (SEM, Hitachi S-4800, Japan); the Brunauer-Emmett-Teller (BET, TriStar 3000 V6.07. The point of zero charge pH_{pzc} was experimentally determined: prepared 10 solutions of 0.1 M KCl with pH in the range of 2 to 11 (pH was adjusted by 0.1 M NaOH and 0.1 M HCl solution). Added 0.025 g LB600 to each 25 ml of the above KCl solution, agitated them for 24 h. The solutions were filtrated and the final pH was measured to determine $\Delta pH = pH_{final} - pH_{initial}$. Plot the ΔpH versus initial pH, the pH_{pzc} was the initial pH which ΔpH is zero.

Adsorption experiment

To conduct experimental adsorption studies, 20 mg L^{-1} DR79 or 10 mg L^{-1} CIP was prepared at determined pH (2, 4, 6, 8, 10) – worked solution (WS). 10 mL of WS was put into 15 mL Facol tube, added 0.01 g LB600, mix the solution well with a shaker for 3 h at room temperature. After that, the WS was centrifuged at 6000 rpm for 10 minutes, collected the solution to determine the concentration of DR79/CIP. The pollutants concentration before (C_o) and after (C_t) adsorption were measured by UV-Vis spectroscopy method at wavelengths of 509 / 276 nm (Agilent Cary 60), with standard curves established within the concentration range of 0.1 to 30 mg/L. Control samples were subjected to the same procedure without pollutants. Each experiment was replicated three times to obtain the mean value. The adsorption and quantification process for pollutants was carried out similarly with different LB600 concentrations (0.5 - 10 g/L), different initial pollutant concentrations (C_o = 5 - 500 mg/L), different times (t = 5-240 minutes), and different temperatures (T = 25-35°C).

The adsorption efficiency and capacity (AE, % and q_t, mg/g) are calculated using the following formulas:

$$AE = \frac{C_o - C_t}{C_o} x100\% \ (\%) \qquad (1)$$

$$q_t = \frac{C_o - C_t}{m} V \ (mg/g) \qquad (2)$$

Where: m is the mass of the adsorbent (g); V is the volume of the WS (L).

The experimental data were analyzed using the Langmuir, Freundlich and Sips adsorption isotherm models according to the equations: [7]:

$$q_e = q_m \frac{K_L C_e}{1 + K_L C_e} \qquad (3)$$

$$q_e = K_F C_e^{n_F} \qquad (4)$$

$$q_e = q_m \frac{K_S C_e^{n_S}}{1 + K_S C_e^{n_S}} \qquad (5)$$

https://doi.org/10.62239/jca.2026.033

Here, q_m was the maximum monolayer adsorption capacity (mg/g). K_L (L/mg), K_F (L/mg), and K_S (L/mg) denote the equilibrium constants as per the Langmuir, Freundlich, and Sips isotherm models, respectively. n_F, n_S are Freundlich and Sips exponents (0<n<1).

Adsorption kinetic was studied through second-order reaction kinetic (SRK), intra-particle diffusion kinetic (ID), and Elovich kinetic models according to the equations [8]:

$$q_t = \frac{k_2 q_e^2 t}{1+k_2 q_e t} \quad (6)$$

$$q_t = k_d t^{0.5} + C \quad (7)$$

$$q_t = \frac{1}{k_e}\ln(a.k_e + t) \quad (8)$$

Where: k_d (mg.g^{-1}.min$^{-0.5}$), k_2 (g.mg^{-1}.min^{-1}) and k_E (g.mg^{-1}) are the rate constants corresponding to the ID, SRK and Elovich models, respectively; C is a parameter within the ID equation and a is initial adsorption rate in Elovich equation. Some thermodynamic parameters can be calculated following equations [9]:

$$K = \frac{q_e}{C_e} \quad (9)$$

$$log\frac{K_{T2}}{K_{T1}} = \frac{\Delta H}{2.303R}.\left(\frac{1}{T_1}\frac{1}{T_2}\right) \quad (10)$$

$$\Delta G = -RT\ln K = \Delta H - T\Delta S \quad (11)$$

where R = 8.314 (J/mol.K), T (Kelvin) is the absolute temperature, C_e (mg/L) is the equilibrium concentration of DR79 on solution. K is equilibrium constant.

Results and discussion

Characterization of the LB600

The pristine biomass (Fig.1a and 1b) exhibits a dense fibrous network with well-preserved cellular structures and limited porosity.

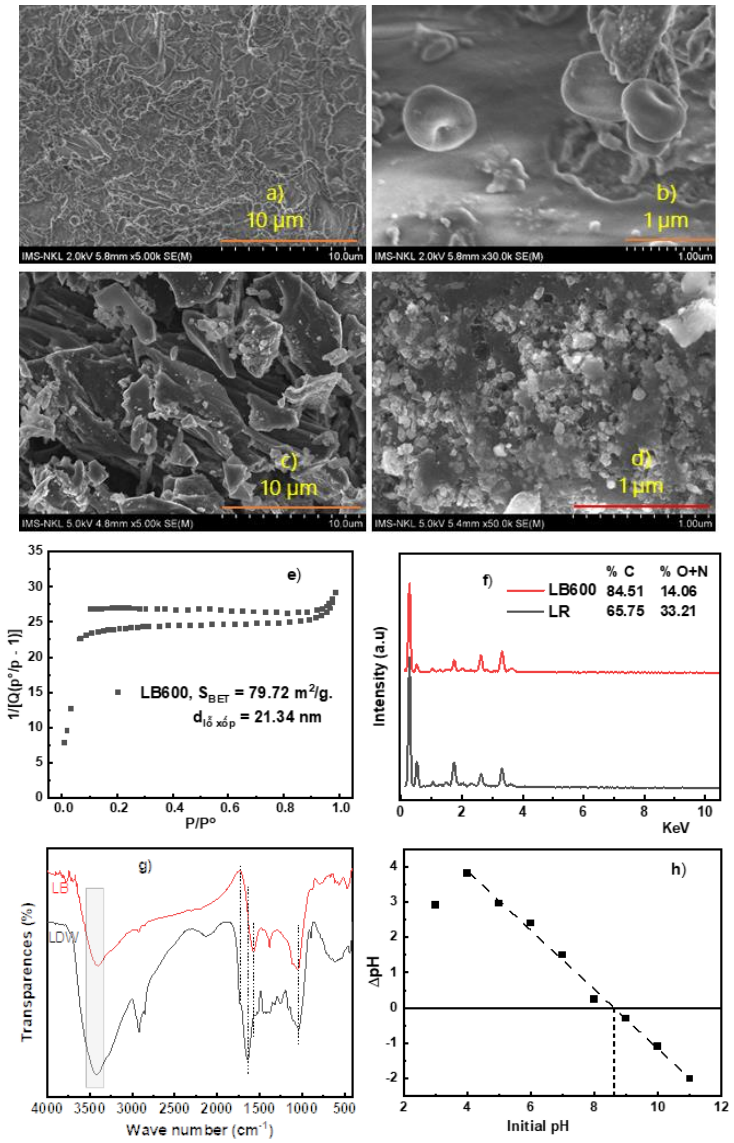


Fig. 1: SEM images of LR (a, b) and LB600 (c, d); (e) BET plot, (f) EDS spectrum, (g) FTIR spectrum & (h) pH_{pzc} plot of LB600

https://doi.org/10.62239/jca.2026.033

After pyrolysis at 600°C for 1 hour, the original biomass structure was largely destroyed by degassing and decomposition of cellulose, hemicellulose, and lignin. The LB600 surface (Fig. 1c and 1d) is rough and heterogeneous, characterized by cracks, cavities, and carbon fragments. Higher magnification images more clearly show the formation of clustered particles and interconnected voids, indicating the development of a porous structure.

The N_2 adsorption-desorption isotherm of the LB600 sample (Fig 1e) shows that, the material has an S_{BET} = 79.72 m^2 g^{-1}, in the medium to fairly high range [10]. The shape of the isotherm is consistent with IUPAC type IV isotherms, commonly found in mesoporous materials, is consistent with a calculated average pore diameter of ~ 21 nm. This mesoporous system is particularly favorable for bulk transport and adsorption of large molecules as azo dyes (DR79) or antibiotics.

EDS spectra and elemental quantification results indicate that the pyrolysis process significantly altered the surface chemical composition of the material (Fig 1f). After pyrolysis at 600 °C (LB600), the carbon content increased sharply (84.51%) compared to the initial biomass (63.75%), while oxygen decreased to only 14.06%. This is a result of dehydration, decarboxylation, and decarbonylation reactions during pyrolysis, transforming the oxygen-rich biomass into a more aromatic carbon-rich network, consistent with the mesoporous system development observed in BET analysis as well as the disruption of plant cell structures in SEM images. The high carbon content and the O/C ratio decreased sharply from about 0.52 to 0.17 after pyrolysis, also suggesting a significant increase in the aromatic/turbostratic carbon domains and chemical stability of the material.

The FTIR spectrum (Fig 1g) provides further evidence of significant chemical alteration following the pyrolysis process: most oxygen-containing functional groups were significantly weakened or disappeared (the O–H stretching band in the 3200–3600 cm^{-1}, the carbonyl group-related bands around 1700 cm^{-1}, the C–O stretching vibration in the 1000–1300 cm^{-1} region [9]), entirely consistent with the decrease in oxygen content from the EDS results. The weak bands of them indicates that some hydroxyl, phenolic, carbonyl, or ether groups remain on the carbon surface.

The pH_{pzc} value determined from Fig. 1h is approximately 8.5–9.0. Such a relatively high pH_{pzc} is commonly observed in highly carbonized biochar and reflects the removal of acidic oxygen-containing groups during pyrolysis. Consequently, the surface is positively charged at pH < 8.5 and negatively charged only at pH > 9.

The CIP/DR79 adsorption behavior of LP600

The adsorption performance of LB600 was strongly affected by the pH of the solution (Fig 2a).

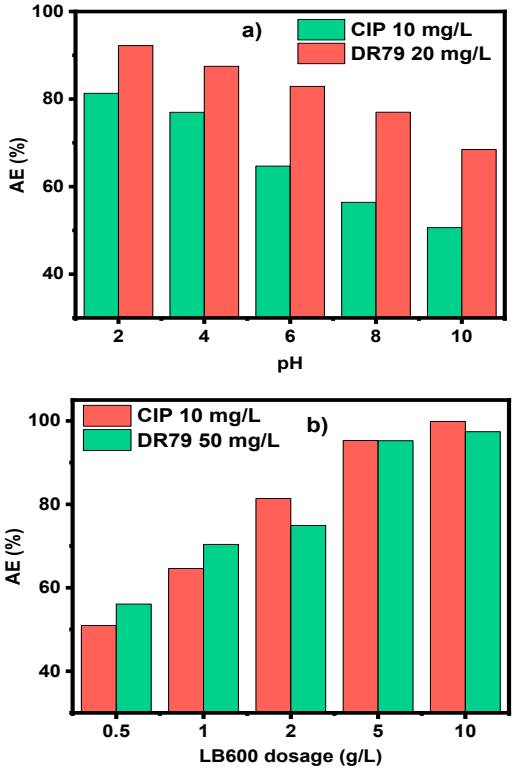


Fig. 2: The effect of pH (a) and adsorbent dose (b) to DR79/CIP adsorption of LB600

For both pollutants, the AE decreased gradually as the pH increased from 2 to 10, and the pH dependence of CIP was more pronounced than that of D79. For CIP, the AE decreased significantly from ~ 81% at pH 2 to ~ 50% at pH 10. CIP exists predominantly as a cationic species at acidic pH, a zwitterion near neutral pH, and an anionic species under alkaline conditions (pKa_1 ≈ 6.1; pKa_2 ≈ 8.7). Since the pH_{pzc} of LB600 is 8.5–9.0, the biochar surface is positive charge as pH decreases, demonstrating that CIP adsorption is not dominated by electrostatic attraction. For DR79, the AE decreased from ~ 92% down to ~ 69% as the pH increased from 2 to 10. Unlike CIP, DR79 is an anionic azo dye containing many sulfonate groups ($–SO_3^-$), meaning that DR79 interacts strongly with the positively charged LB600 surface under acidic conditions, significantly influenced by electrostatic attraction. However, the relatively moderate decrease suggests that the contribution of non-electrostatic interactions, particularly π–π interactions, still play a significant role over a wide pH range.

https://doi.org/10.62239/jca.2026.033

The effect of LB600 dosage on the adsorption of CIP and DR79 at pH 2 is shown in Fig. 2b. Increasing the adsorbent dosage from 0.5 to 5 g/L significantly enhanced the removal efficiency of both pollutants: from ~ 51% to nearly 100% for CIP and from ~ 56% to about 97% for DR79. This improvement may be due to an increased number of adsorption sites. The rapid increase in efficiency for CIP compared to DR79 indicates that the space and bulky structure of DR79 significantly affect the AE. At concentrations of 5 to 10 g/L, the improvement was negligible, suggesting that adsorption equilibrium was almost reached.

Adsorption isothermal:

The effect of C_o (DR79, CIP) on q_e and the modeling of experimental data using different adsorption isotherms are shown in Fig 3.

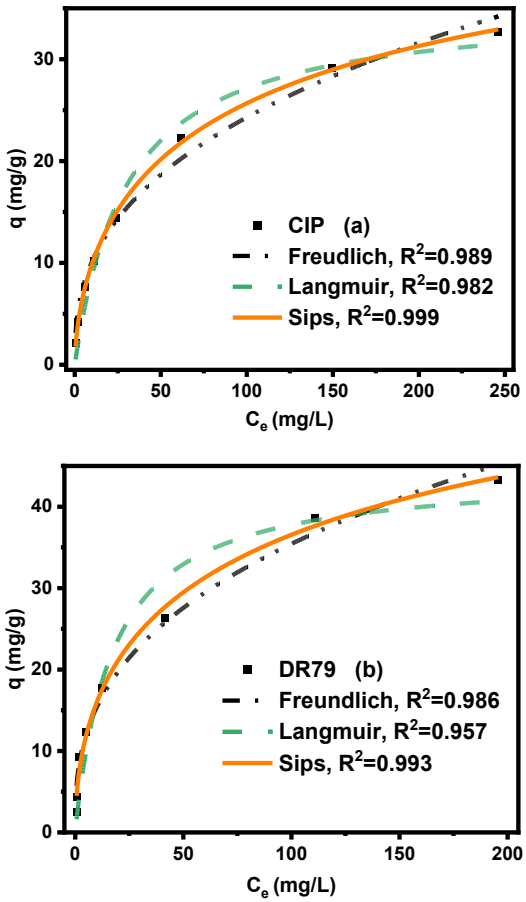


Fig. 3: The effect of initial pollutant concentration on adsorption capacity and the modeling of experimental data using different adsorption isotherms

The $q_{e,exp}$ for both CIP and DR79 increase continuously with pollutant C_o, the $q_{m,exp}$ reaches approximately 33–34 mg g^{-1} for CIP and 44–45 mg g^{-1} for DR79, suggesting a stronger overall affinity of LB600 toward DR79 than CIP. q_m is average compared with several other studies (Table 1). The higher q_m of DR79 compared to CIP can be attributed to the stronger and more diverse affinity of the dye molecules toward the porous aromatic carbon framework of LB600 (involving multiple aromatic rings, azo linkages, hydroxyl groups, and sulfonate groups). In contrast, CIP contains only a relatively small quinolone ring system, so its π–π interaction is usually significantly weaker, the electrostatic repulsion between the LP600 surface and the CIP cation at pH2 also reduced the q_{CIP}.

Table 1: CIP/DR79 adsorption capacity of some biochar

No.	Biochar	$q_{m,CIP}$	$q_{m,DR79}$	Ref.
1	Pine bark	26.61		[11]
2	Rice straw	3.71		[12]
	H_3PO_4 modified	8.77		
	KOH-modofied	25.6		
3	Modified bamboo	78.43		[13]
4	Modified Birch sawdust	86.26		[14]
5	EDTA-modified Bellamya shell		10.78	[15]
6	CTAB-modified natural laterite		55.95	[16]
7	NaOH-modified longan seed		684.93	[5]
8	Lemongrass	33	44	This study

The R^2 of all three models were very high, from 0.957 to 0.999, with the Sips model having the highest value. This indicates that the CIP/DR79 adsorption process takes place on a heterogeneous surface. And Freundlich performs substantially better than Langmuir indicates that the adsorption energy is not uniform, the surface has many types of adsorption sites, and adsorption occurs simultaneously through several different adsorption mechanisms, such as π–π stacking, hydrogen bonding, electrostatic attraction and pore-filling effects [7].

Adsorption kinetic:

The effect of time and temperature on adsorption capacity and the modeling of experimental data using different adsorption kinetic models are shown in Fig 4.

Both DR79 and CIP adsorption occurs rapidly in the initial phase (5–15 minutes), then slows down until equilibrium, but DR79 reaches equilibrium faster than CIP. As temperature increase from 20 to 40 °C, the $q_{e,CIP}$ increased from 8.21 to 8.50 mg/g, while $q_{e,DR79}$ decreased from about 9.67 to 9.60 mg/g. This demonstrates that for large molecules like DR79,

https://doi.org/10.62239/jca.2026.033

increased temperature motion weakens their interaction with the adsorbent, while smaller CIP molecules can enhance pore-filling motion, leading to increased adsorption capacity.

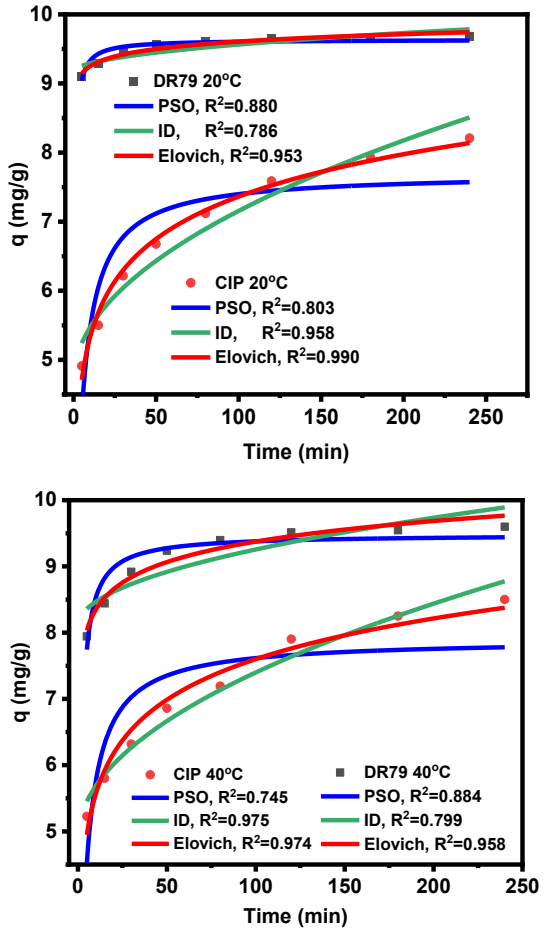


Fig. 4: The effect of time and temperature on adsorption capacity and the modeling of experimental data using different adsorption kinetic models

For DR79, the Elovich model consistently provides the best fit at both temperatures (R^2 ≈ 0.95–0.96), whereas the PSO and ID models exhibits poor agreement. It indicates that adsorption occurs on a highly heterogeneous surface with a broad distribution of activation energies [8]. Unlike DR79, CIP exhibits excellent fitting with both the Elovich and ID models. At 20 °C, Elovich gives the highest R^2 (0.990), whereas at 40 °C both Elovich (0.974) and ID (0.975) describe the data equally well. These results indicate that CIP adsorption involves two coupled processes: adsorption on energetically heterogeneous surface sites and diffusion into the internal pore structure. The smaller molecular size of CIP compared with DR79 allows it to penetrate more deeply into the porous network of LB600. Consequently, pore transport limitations become more evident for CIP than for DR79 [9]. The moderate fit of the PSO model suggests that although surface interactions are important, adsorption is more complex than a single chemisorption mechanism [8]. Some adsorption parameters are shown on Table 2.

Table 2: Some thermodynamic parameters of adsorption

Parameters	CIP adsorption	DR79 adsorption
$q_{m,\,exp}$ (mg/g)	32.69	43.35
$q_{m,\,cal}$ (mg/g)	35.36	44.27
K_{20} (L/g)	4.583	6.556
K_{40} (L/g)	5.674	5.903
ΔG_{20} (kJ/mol)	-3.71	-4.58
ΔG_{40} (kJ/mol)	-4.23	-4.62
ΔH (kJ/mol)	8.14	-4.00
ΔS_{20} (J/mol.K)	40.43	1.98
ΔS_{40} (J/mol.K)	39.51	1.98

Table 2 shows that the adsorption processes all occurred spontaneously within the investigated temperature range. At the same time, ΔG_{DR79} were more negative than ΔG_{CIP}, K_{DR79} were also larger, indicating that DR79 has a stronger thermodynamic affinity for LB600 than CIP, consistent with $q_{m.DR79}$ being larger than $q_{m.CIP}$. The CIP adsorption process is endothermic, while the DR79 adsorption process is exothermic. Higher temperatures generally increase ID, reduce hydration resistance, and improve accessibility to adsorption sites within the capillary. These enthalpy results are in full agreement with how the ID model very well describes the CIP adsorption process. The entropy changes of the adsorption processes were all positive, but for the CIP adsorption was quite large (~40 J/mol/K), indicating that although CIP was retained on the surface, the number of water molecules due to dehydration was greater than the loss of CIP's freedom of movement. Meanwhile, the entropy of the DR79 adsorption process was quite small, suggesting that structural rearrangement of the system was almost negligible, with adsorption mainly occurring through pre-existing interactions within the structure. The low absolute ΔH values indicate that adsorption of both pollutants is dominated by physical interactions.

Conclusion

The pyrolysis process at 600°C for 1 hour transformed the dense lignocellulosic structure of the lemongrass biomass into a developed mesoporous carbon

network, forming cracks, voids, and interconnected capillaries with a specific surface area of approximately 79 m^2/g and an average pore diameter of about 21 nm. EDS and FTIR analysis demonstrated strong carbonization, forming aromatic carbon domains while maintaining an appropriate amount of hydroxyl, carbonyl, and ether groups on the surface. LP600 adsorbed DR79 better than CIP ($q_{e,DR79}$ ~ 44 mg/g, $q_{e,CIP}$ ~33 mg/g). The adsorption of DR79 mainly occurs via electrostatic attraction, π–π interactions between the dye and aromatic carbon domains; hydrogen bonding and pore-filling mechanisms in the mesoporous system. Meanwhile, the adsorption of CIP is controlled by hydrogen bonding, intracellular diffusion in the capillary network and possibly partly by π–π interactions and acid–base interactions. Thus, the pyrolysis of lemongrass residue at 600°C produces a mesoporous carbon material that effectively treats water contaminated by both antibiotics and dyes of varying structures, opening up potential applications in the treatment of complex wastewater systems. This also provides an important basis for the development of inexpensive, sustainable, and environmentally friendly biochar materials from agricultural by-products for next-generation water treatment technologies.

References

1. Y. Trivedi, M. Sharma, R.K. Mishra, A. Sharma, J. Joshi, A.B. Gupta, B. Achintya, K. Shah, A.K. Vuppaladadiyamd, Desalination, 600 (2025) 118509. https://doi.org/10.1016/j.desal.2024.118509
2. T.T. Truong, T.X. Vuong, T.H.H. Chu, T.H.T. Diep, H.C. Ta, L.P. Hoang, T.D. Pham, J. Water Process Eng., 71 (2025) 107402. https://doi.org/10.1016/j.jwpe.2025.107402
3. T.T.U. Le, T.G. Ngo, N.A. Hoang, V.H. Nguyen, V.D. Nguyen, L.P. Hoang, T.D. Pham, T.T. Truong, J. Mol. Liq., 425 (2025) 127205. https://doi.org/10.1016/j.molliq.2025.127205
4. V.S.R. Bisi, W.P. Silvestre, M.H. Tramontin, E.D. Conte, M. Godinho, G.F. Pauletti, Int. J. Recycl. Org. Waste Agric., 13(5) (2024). https://doi.org/10.57647/ijrowa-zetg-p321
5. B.M. Al-howri, S. Ismail, M. Khajavian, Environ. Monit. Assess., 197 (2025) 1095. https://doi.org/10.1007/s10661-025-14454-z
6. V.T. Hau, TNU J. Sci. Technol., 229(10) (2024) 228-237. https://doi.org/10.34238/tnu-jst.9908
7. X. Wang, Q. Zhang, Minerals, 10 (2020) 114. https://doi.org/10.3390/min10020114
8. J. Wang, X. Guo, J. Hazard. Mater., 390 (2020) 122156. https://doi.org/10.1016/j.jhazmat.2020.122156
9. X. Zhou, X. Yu, R. Maimaitiniyazi, X. Zhang, Q. Qu, Heliyon, 10(8) (2024) e28188. https://doi.org/10.1016/j.heliyon.2024.e28188
10. T.U. Vandana, B.K. Tripathy, R.K. Mishra, A. Sharma, K. Mohanty, Process Saf. Environ. Prot., 210 (2025) 107505. https://doi.org/10.1016/j.psep.2025.107505
11. H.P. Thao, N.H. Ha, T.T.H. Linh, L.V.T. Anh, N.T.T. Uyen, V.T.B. Ngoc, N.P. Ho, Vietnam J. Catal. Adsorpt., 14(3) (2025) 23-29. https://doi.org/10.62239/jca.2025.033
12. H. Wang, H. Wang, S. Shahab, H. Cheng, M. Atroshko, X. Wang, M. Ye, Results Chem., 17 (2025) 102603. https://doi.org/10.1016/j.rechem.2025.102603
13. W.K. Wakejo, B.T. Meshasha, J.W. Kang, Y. Chebude, Adsorpt. Sci. Technol., 2022 (2022) 2699530. https://doi.org/10.1155/2022/2699530
14. F. Shen, S. Liu, Z. Liu, J. Wei, M. Huang, J. He, Y. Zhang, J. Hu, D. Tian, F. Shen, Chin. J. Chem. Eng., (2025). https://doi.org/10.1016/j.cjche.2025.08.019
15. T.M.V. Ngo, T.T.L. Nguyen, X.T. Mai, T.T.A. Duong, V.N. Vu, T.H. Vu, T.D. Pham, Int. J. Environ. Sci. Technol., 22 (2025) 15857-15870. https://doi.org/10.1007/s13762-025-06703-y
16. T.N.A. Tuyet, V.T. Hau, TNU J. Sci. Technol., 230 (2025) 61-71. https://doi.org/10.34238/tnu-jst.13171